A direct forcing immersed boundary method for simulating floating objects

A. Soydan, W. Wang, A. Kamath & H. Bihs
Norwegian University of Science and Technology, NTNU, Trondheim

ABSTRACT: For ship and offshore applications, the fluid-floating object interaction is of particular importance and accurate numerical calculations are required. However, low-order accurate methods are not sufficient to have decent results even though they are computationally efficient. Therefore, high-resolution fluid-floating body coupling modeling is still needed in computational fluid dynamics (CFD) based solvers. In this study, the capability of a direct forcing immersed boundary approach to model a floating object in fluid domain is investigated. This method is implemented to be able to handle rigid-body motion within the high-resolution computational fluid dynamics (CFD) solver REEF3D::CFD which is used for numerical calculations. The validation study includes the heave motion tests of a three-dimensional buoy. Here, the free surface is calculated with the level set method, convection terms are discretized with fifth-order WENO schemes, and a third-order TVD Runge-Kutta scheme. The numerical results are compared with the available data in the literature.

1 INTRODUCTION

Fluid-structure interaction problems in the marine and coastal engineering fields are even more challenging due to the complex hydrodynamic behavior of the free surface. With the advances of the Computational Fluid Dynamics (CFD) algorithms, the complex nonlinear fluid-floating object interaction problems can be calculated by solving the Reynolds-averaged Navier-Stokes equations. Nevertheless, efficient and accurate numerical tools are still needed and various research is devoted to contributing to a better understanding of the fluid-floating object interaction, particularly in wave conditions.

The recent research addresses the numerical modeling of rigid body motion in the fluid domain and loads&stresses on the structure which are crucial for determining the safety of the structure under certain conditions. Kamath et al. (2016) used REEF3D::CFD model to calculate the interaction between breaking wave and a vertical cylinder. The numerical results were compared with experimental data numerical findings show that the model can be used for wave-structure interaction. Similar structure was used under regular and irregular waves conditions to calculate breaking forces by Alagan Chella et al. (2017) and Aggarwal et al. (2017). A high-resolution two-phase flow solver was developed by Calderer et al. (2018) to carry out floating offshore structures interaction with realistic sea conditions. The solver uses a high-order spectral method with a level set method to model airflow and waves. Similarly, Liu et al. (2017) also investigated a floating offshore wind turbine under wind and wave conditions using OpenFOAM. Islam and Guedes Soares (2020) carried out a validation study for free heave decay test and heave decay test under regular wave conditions with a sphere using OpenFOAM. The numerical results were compared with the numerical results of the other research groups.

In this study, a heaving sphere is investigated using the CFD code REEF3D (Bihs et al. 2016). REEF3D is an open-source hydrodynamic framework being developed at NTNU with a focus on wave hydrodynamics and coastal and marine applications. A continuous direct-forcing method is implemented to handle fluid-rigid body interaction and three-dimensional applications were already carried out (Martin et al. 2021, Wang et al. 2022). In order to assess the capability of the current rigid-body motion algorithm,it is tested with a buoy case similar to study of Islam and Guedes Soares (2020). The numerical results obtained from REEF3D is compared with the other results available in the literature.

2 NUMERICAL METHODS

2.1 *Governing Equations*

The conservation of mass and momentum which are written in compact tensor notation should be satisfied for an incompressible fluid.

$$\frac{\partial u_i}{\partial x_i} = 0 \tag{1}$$

$$\frac{\partial u_i}{\partial t} + u_j \frac{\partial u_i}{\partial x_j} = -\frac{1}{\rho}\frac{\partial p}{\partial x_i} + \frac{\partial}{\partial x_j}\left[(\nu + \nu_t)\left(\frac{\partial u_i}{\partial x_j} + \frac{\partial u_j}{\partial x_i}\right)\right] + g_i \tag{2}$$

Here, u is the velocity, ρ is the density of the fluid, p is the pressure, ν is the kinematic viscosity, ν_t is the eddy viscosity and g_i the acceleration vector due to gravity and it is valid only in the z-direction. In REEF3D::CFD, the two-equation $k-\omega$ turbulence model is implemented (Wilcox 1994). The eddy viscosity ν_t is calculated from the turbulent kinetic energy k and specific turbulent dissipation rate ω as $\nu_t = k/\omega$. The k and ω equations are defined as follows:

$$\frac{\partial k}{\partial t} + u_j \frac{\partial k}{\partial x_j} = \frac{\partial}{\partial x_j}\left[\left(\nu + \frac{\nu_t}{\sigma_k}\right)\frac{\partial k}{\partial x_j} +\right] + P_k - \beta_k k\omega \tag{3}$$

$$\frac{\partial \omega}{\partial t} + u_j \frac{\partial \omega}{\partial x_j} = \frac{\partial}{\partial x_j}\left[\left(\nu + \frac{\nu_t}{\sigma_w}\right)\frac{\partial w}{\partial x_j} +\right] + \frac{\omega}{k}\alpha P_k - \beta\omega^2 \tag{4}$$

where P_k is the turbulent production rate, and the coefficients have the values $\alpha = \frac{5}{9}, \beta_k = \frac{9}{100}, \beta = \frac{3}{40}, \sigma_k = 2$ and $\sigma_\omega = 2$. This turbulence model is suitable for unsteady two-phase fluid problems as shown in (Kamath et al. 2019) because of the linear relationship between k and ω. A limiter for the eddy viscosity is taken into account to avoid over-production of turbulence in highly strained flows outside the boundary layer (Durbin 2009):

$$v_t = min\left(\frac{k}{\omega}, \sqrt{\frac{2}{3}}\frac{k}{|\mathbf{S}|}\right) \tag{5}$$

where $|\mathbf{S}|$ is the magnitude of the strain tensor. Due to the reduced turbulent length scales, turbulence dissipation is increased in the vicinity of the free surface. Also, the turbulence fluctuations are damped normal to the free surface and this leads to enhanced intensity parallel to the free surface. Through the implementation of the following additional turbulence damping boundary condition (Naot & Rodi 1982) at the free surface, this behavior can be included in the turbulence model with the specific turbulent dissipation ω_S at the free surface:

$$\omega_s = \frac{c_\mu^{-\frac{1}{4}}}{\kappa} k^{\frac{1}{2}} \cdot \left(\frac{1}{y'} + \frac{1}{y^*}\right) \tag{6}$$

where $C_\mu = 0.07$ and $\kappa = 0.4$.The variable y' is the virtual origin of the turbulent length scale, and was empirically found to be 0.07 times the mean water depth (Hossain & Rodi 1980). Including the distance y^* from the nearest wall gives a smooth transition from the free surface value to the wall boundary value of ω. Aforementioned damping is activated only around the interface with the Dirac delta function $\delta(\phi)$:

$$\delta(\phi) = \begin{cases} \frac{1}{2\epsilon}\left(1 + \cos\left(\frac{\pi\phi}{\epsilon}\right)\right) & \text{if } |\phi| < \epsilon \\ 0 & \text{else} \end{cases} \tag{7}$$

where $\epsilon = 1.6\Delta x$ and Δx is the grid size.

2.2 *Free surface representation*

For the transition between the air and water phases ,the level set function is (Osher & Sethian 1988) used,which is defined as a signed distance function:

$$\Phi(\vec{x}, t) = \begin{cases} > 0 & \text{if } \vec{x} \in \text{phase 1} \\ = 0 & \text{if } \vec{x} \in \Gamma \\ < 0 & \text{if } \vec{x} \in \text{phase 2} \end{cases} \tag{8}$$

The Eikonal equation $|\nabla\Phi| = 1$ should also be satisfied in order to ensure mass conservation. A convection equation for the level set function

$$\frac{\partial \Phi}{\partial t} + u_j \frac{\partial \Phi}{\partial x_j} = 0 \tag{9}$$

is solved using the fluid velocity field u. The level set function is reinitialized after each time step to keep the signed distance proporties. In REEF3D, a PDE based reinitializion equation is solved (Sussman et al. 1994):

$$\frac{\partial \Phi}{\partial t} + S(\Phi)\left(\left|\frac{\partial \Phi}{\partial x_j}\right| - 1\right) = 0 \tag{10}$$

where $S(\Phi)$ is the smoothed sign function (Peng et al. 1999). And then, the density and viscosity is calculated using

$$\rho = \rho_w H(\Phi) + \rho_a(1 - H(\Phi)) \tag{11}$$

$$\nu = \nu_w H(\Phi) + \nu_a(1 - H(\Phi)) \tag{12}$$

Here, w and a indicate water and air properties, respectively. The following Heaviside step function

$H(\Phi)$ is used for smoothing of the sharp change of the fluid properties at the interface

$$H(\Phi) = \begin{cases} = 0 & \text{if } \Phi < -\epsilon \\ = \frac{1}{2}\left(1 + \frac{\Phi}{\epsilon} + \frac{1}{\pi}\sin\left(\frac{\pi\Phi}{\epsilon}\right)\right) & \text{if } |\Phi| \leq -\epsilon \\ = 1 & \text{if } \Phi < \epsilon \end{cases} \tag{13}$$

with an interface thickness of $\epsilon = 2.1\Delta x$.

2.3 *Numerical schemes*

The system of equations is solved using finite differences on a rectilinear staggered grid. A fifth-order accurate weighted essentially non-oscillatory (WENO) scheme (Jiang & Shu 1996) is applied for the convection terms. The fifth-order accurate Hamilton-Jacobi WENO method of (Jiang & Peng 2000) is used for discretization of the convection term in eq. (9). For diffusion terms, the second-order accurate central finite difference scheme is applied. An incremental pressure-correction algorithm (Timmermans et al. 1996) is used for the solution of the pressure gradient term in the RANS equation as described in (Martin et al. 2021). In the predictor step, the conservation equation for momentum eq. (2) is solved without considering the pressure gradients. An intermediate velocity field $u_i^{(*)}$ is calculated in each k-th Runge-Kutta sub-step using the following equation:

$$\frac{u_i^{(*)} - \alpha_k u_i^{(n)}}{\alpha_k \Delta t} = \frac{\beta_k}{\alpha_k} u_i^{(k-1)} - u_j^{(k-1)} \frac{\partial u_i^{(k-1)}}{\partial x_j} - \frac{1}{\rho}\frac{\partial p^{(k-1)}}{\partial x_i} + \frac{\partial}{\partial x_j}\left(\nu \cdot \left(\frac{\partial u_i}{\partial x_j} + \frac{\partial u_j}{\partial x_i}\right)\right)^{(*)} + g_i \tag{14}$$

Here, α_k =1.0, 1/4, 2/3, β_k =0.0, 3/4,1/3 and k =1, 2, 3. The third-order accurate Total Variation Diminishing (TVD) Runge-Kutta scheme (Shu & Osher 1988) is applied for the solution of the time derivatives as well as for eq. (9) and eq. (10). The time step size is controlled under the restriction of the CFL condition to ensure numerical stability efficiently. An implicit Euler method is applied for the time advancement of k and ω equations to prevent a significantly smaller time step size due to the CFL criterion. More detail can be found in (Bihs et al. 2016). Diffusion term of the RANS equation is treated implicitly to remove their CFL restriction. The Poisson equation for the pressure of the new time step is formed by the insertion of the predicted velocities into the continuity equation.

$$\frac{\partial}{\partial x_i}\left(\frac{1}{\rho}\frac{\partial p_{corr}}{\partial x_i}\right) = \frac{1}{\alpha_k \Delta t}\frac{\partial u_i^*}{\partial x_i} \tag{15}$$

The Poisson equation is solved for the pressure correction terms p_{corr} by the fully parallelized BiCGStab algorithm of the HYPRE library (van der Vorst 1992) with the geometric multigrid pre-conditioner (Ashby & Flagout 1996) to increase the computational performance. Finally, the pressure and divergence-free velocity field are calculated using the following equations:

$$p^{(k)} = p^{(k-1)} + p_{corr} - \rho\nu\frac{\partial u_i^*}{\partial x_i} \tag{16}$$

$$u_i^{(k)} = u_i^* - \frac{\alpha_k \Delta t}{\rho}\frac{\partial p^{(k)}}{\partial x_i} \tag{17}$$

2.4 *Rigid Body-Fluid Interaction*

To calculate rigid-body motion in the Eulerian fluid domain, a continuous direct forcing method is available in REEF3D (Martin et al. 2021). A floating object can be represented with an STL geometry consisting of multiple non-connected triangles. A ray casting algorithm (Bihs et al. 2017) is utilized to get inside-outside information in the vicinity of the body. Thus a signed distance function Φ_s can be generated. Eq. (11) and eq. (12) are extended to distinguish between fluid and solid domain.

$$\rho = \rho_s H(\Phi_s) + (1 - H(\Phi_s)) \cdot (\rho_w H(\Phi) + \rho_a(1 - H(\Phi)) \tag{18}$$

$$\nu = (1 - H(\Phi_s)) \cdot (\nu_w H(\Phi) + \nu_a(1 - H(\Phi))) \tag{19}$$

Here, s indicates solid and $H(\Phi_s)$ is used for representing the transition of fluid to solid. A direct-forcing method is used to couple the solid and fluid domain. Here, the additional source term **f** is included in the momentum equations to ensure the correct boundary conditions at the interface. Following the derivation in (Yang 2018), the following term is added to the predicted momentum. After the predictor step, smoothed **f** can be calculated as follows:

$$\mathbf{f}^{(*)} = H\left(\Phi_s^{(*)}\right) \cdot \left(\frac{\mathbf{P}(\mathbf{u})^{(*)} - \mathbf{u}^*}{\alpha_k \Delta t}\right) \tag{20}$$

The body forces and moments are calculated on the STL surface using an integration over all N triangles:

$$F_x = \int_\Omega (-\mathbf{n}p + \rho\nu\mathbf{n}\tau) d\Omega(\mathbf{x}) = \sum_{i=1}^{N} (-\mathbf{n}p + \rho\nu\mathbf{n}\tau)_i \cdot \Delta\Omega_i \tag{21}$$

$$M_x = \int_\Omega \mathbf{r} \times (-\mathbf{n}p + \rho\nu\mathbf{n}\tau) d\Omega(\mathbf{x}) \\ = \sum_{i=1}^{N} \mathbf{r}_i \times (-\mathbf{n}p + \rho\nu\mathbf{n}\tau)_i \cdot \Delta\Omega_i \tag{22}$$

Here, $\mathbf{n}$ is the surface normal vector, τ is the viscous stress tensor and $\mathbf{r}$ represents the distance vector to the centre of gravity. Further information about implementation and applications of the continuous direct forcing method can be found in (Martin et al. 2021) and (Wang et al. 2022).

3 RESULTS

3.1 *Heave Decay Simulations*

In this part of the study, heave decay test are carried out for a sphere in order to investigate the capability of a direct forcing immersed boundary method within REEF3D::CFD (Martin et al. 2021). The simulations conditions are taken into account based on a study of literature (Wendt et al. 2017, Islam and Guedes Soares 2020). The general characteristics of the sphere are given in Table 1 and natural draft position of the sphere in the z-direction is 0 m. 2 different initial displacement (1.0 m and 5.0 m) are performed for free-decay test. The simulation domain of the numerical wave tank (NWT) is generated 10 times of the sphere diameter along the x and y direction and 6 times along the z direction. Grid stretching is applied around the sphere in order to represent of the sphere properly which can be seen in Figure 1.

Table 1: General characteristics of the sphere.

Parameters	Specifications
Sphere radius	5.0 m
Sphere origin	0.0, 0.0, 0.0 m
Center of gravity	0.0, 0.0, -2.0 m
Mass of the sphere	261.8 x 10^3
Water depth	Infitinite
Water density	1000 kg/m^3

The free-decay test with 1.0 m initial displacement was simulated for 25 s. Three different mesh size is used as D/25, D/50 and D/100 where D is the diameter of the sphere. CFL number is kept as 0.1 throughout this study. For this reason, temporal convergence is not considered. For heave decay simulations, the results were adjusted to zero level same as the results in Islam and Guedes Soares (2020) for proper comparison. Figure 2 shows the heave motion time history for the case with 1.0 m initial displacement. The mesh size of D/25 shows to differ after the first peak of the heave motion. The mesh sizes of D/50 and D/100 are slightly different from each other and show good agreement with results of Islam and Guedes Soares (2020) until 10.0s. After that, the motions start to differ. For better representation of the sphere mesh size of D/100 will be used for all simulations. Figure 4 shows the heave motion time history where the black line represents REEF3D::CFD results and the red line represents the result in the study of (Islam and Guedes Soares 2020). The other available numerical results in literature also can be seen in Figure 3 and 5. While the result from 1 m initial displacement shows good agreement with that the results from the other research groups, there is a clear discrepancy between the results for the case with 5 m initial displacement. Numerical results show that REEF3D::CFD predicts smaller motion amplitude than the other codes and the motion amplitude damped quickly. It is known

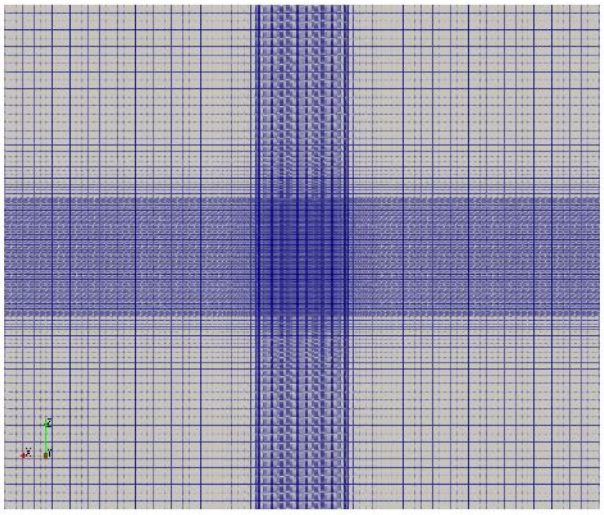

Figure 1: Computational grid for heave decay simulations.

that added mass and hydrodynamic damping, which are proportional to the velocity, are functions of the frequency of oscillatory motion. In this study, a continuous direct forcing method is used to calculate rigid body motion. In this method, the forcing term is calculated on the fluid-solid body interface and a smoothed Heaviside step function is used to transfer quantities between Lagrangian end Eulerian domain. This smoothing process may smear fluid-solid body interface and the tangential velocity in the vicinity of the solid body can be problematic. As a result, the natural frequency damped quickly, especially for the case with 5 m initial displacement, may have been caused by the aforementioned reason. This issue with the continuous direct forcing immersed boundary method is still under investigation and further improvements will be carried out.

To further investigation of the results, the horizontal velocity distribution on the lateral section (Figure 7) and vertical velocity distribution on the free-surface (Figure 8) are given. REEF3D is able to capture higher-order wave radiation effects (Figure 8) and overtopping of water (Figure 7 which are created by the instantaneous sphere cross-section area at the first oscillation of the free-decay motion, particularly. In addition, REEF3D captures the breaking radiated waves (Figure 6) around the sphere clearly.

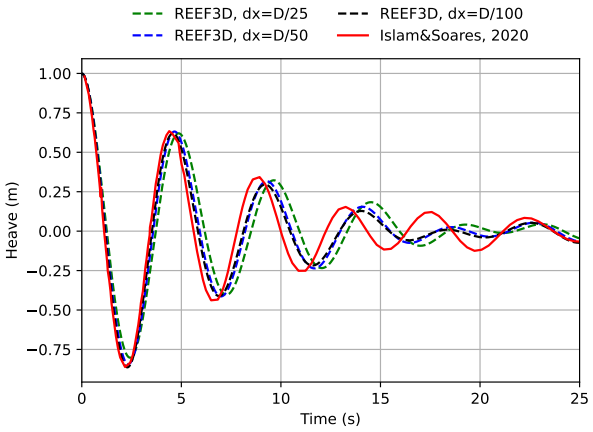

Figure 2: Comparison of heave motions of a sphere with 1.0 m initial displacement.

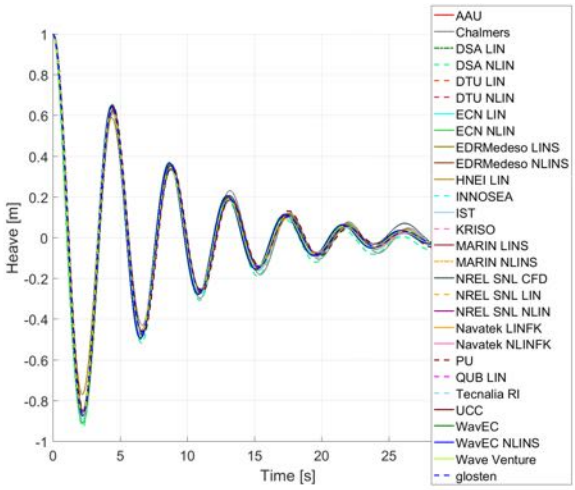

Figure 3: Heave motions of a sphere with 1.0 m initial displacement from literature Wendt et al. (2017).

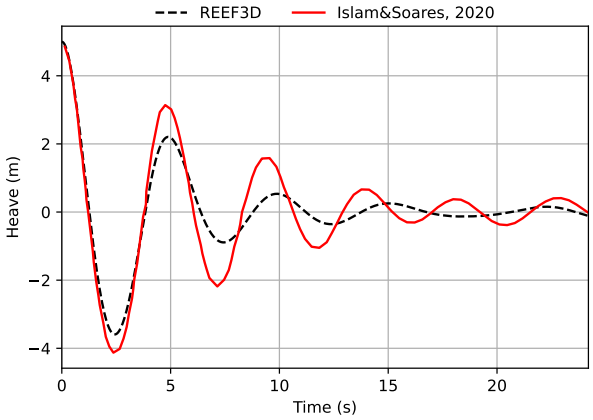

Figure 4: Comparison of heave motions of a sphere with 5.0 m initial displacement.

3.2 *Heave Motions in Regular Wave Conditions*

A floating sphere is simulated under regular wave conditions based on the work of Islam and Guedes Soares (2020). In that work, three different wave steepness are considered as 0.0005, 0.0020 and 0.0100. For validation purpose, only 2 case are carried out for a moderate wave steepness of 0.002. Here, only the heave motion of the sphere are considered. The length of the numerical wave tank (NWT) is chosen depending on the wave length. Several wave gen-

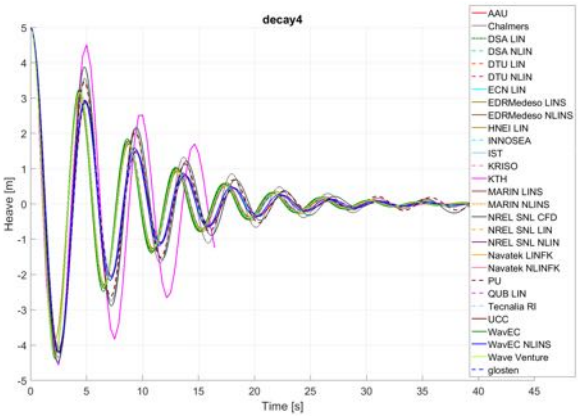

Figure 5: Heave motions of a sphere with 5.0 m initial displacement from literature Wendt et al. (2017).

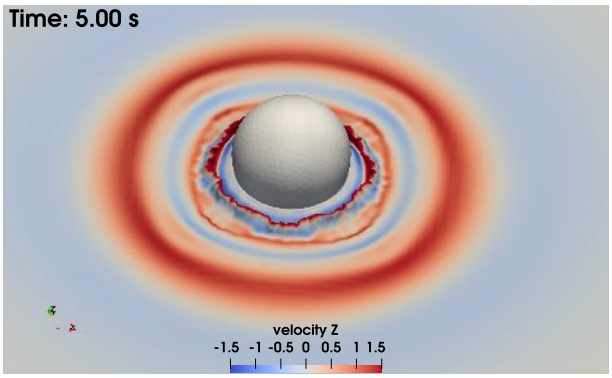

Figure 6: Breaking radiated waves for the case with 5.0 m initial displacement.

eration and absorption methods are included such as the relaxation method, the Dirichlet-type method, and the active wave absorption method within REEF3D numerical framework (Miquel et al. 2018). In this study, the relaxation method is used for both the wave generation and absorption and the wave generation absorption beach is equivalent to one wavelength. 2nd-order Stokes theory is used for the waves. Computational domain and grid stretching which is applied around the sphere can be seen in Figure 9. The heave motion Response Amplitude Operator (RAO) for the sphere is shown in Table 2. The RAO is calculated as follows:

$$RAO = \sqrt{m_{peak}/\zeta_{peak}} \tag{23}$$

where m_{peak} is the first-order peak of the heave motion power spectral density (PSD) and ζ_{peak} is the first order peak of the wave elevation PSD. The simulation conditions which is considered in this study and comparison of RAO value are given in Table 2. In addition, the time history of for heave motion for the wave period of 3.0 s and 7.0 s are given in Fig. 10 and Fig. 12, respectively.Additionally, the spectral analysis of the heave motion for both incident waves are shown in Fig. 11 and Fig. 13. For the 3.0 s wave period, the heave motion response is irregular and numerical results show differences at some peaks. The high-order strong responses in the heave motion for the 3.0 s wave period is also clearly seen in Fig. 11. There is a noticeable second-order peak at about 0.35

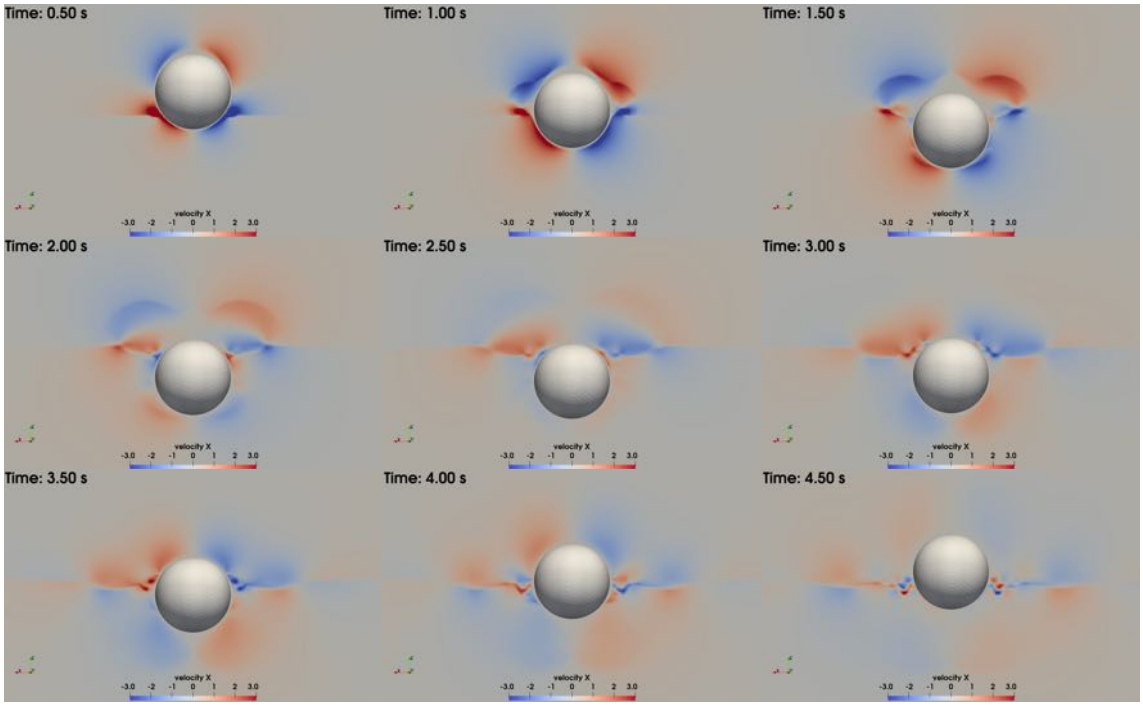

Figure 7: Horizontal velocity distributions on lateral section.

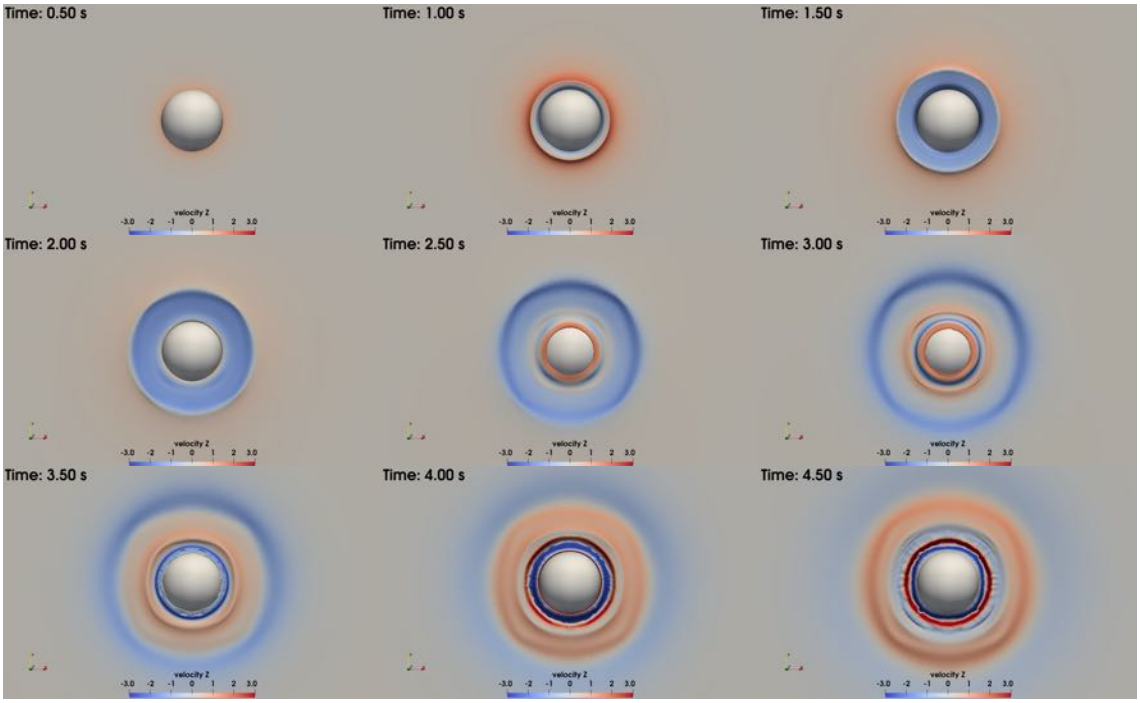

Figure 8: Vertical velocity distributions on free-surface.

Hz for the 3.0 s wave period. Furthermore, the sinkage can be clearly observed for the first incident wave in Fig. 10 since the initial center of gravity of the sphere in the z-direction is at -2 meters. This result is plausible because, in the low wave period, the sphere and the radiated waves from the sphere encounter more with the incoming waves and this can increase the nonlinearities which may cause to change in the relative position between the instantaneous free-surface and heaving sphere.

On the other hand, heave motion response obtained from REEF3D for the wave period of 7.0 s is quite similar to the result of Islam and Guedes Soares (2020). Additionally, the spectral analysis result is given in Fig. 13 and ROA results are too close each other which can be seen in Table 2.

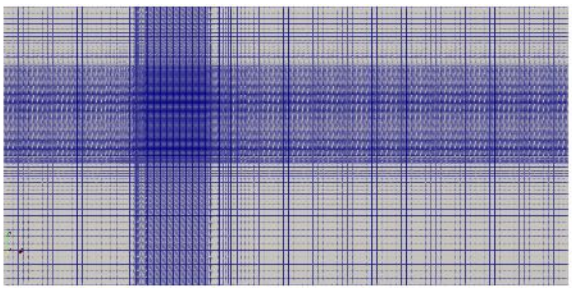

Figure 9: Computational grid for wave simulations.

Table 2: Result of the sphere in regular wave conditions.

Wave Period T (s)	Wave Lenght $\lambda(m)$	Wave Height H (m)	Wave Steepness (S)	RAO (REEF3D)	RAO (Islam and Soares 2020)
3.0	14.04	0.177	0.0020	0.147	0.136
7.0	76.44	0.961	0.0020	1.092	1.14

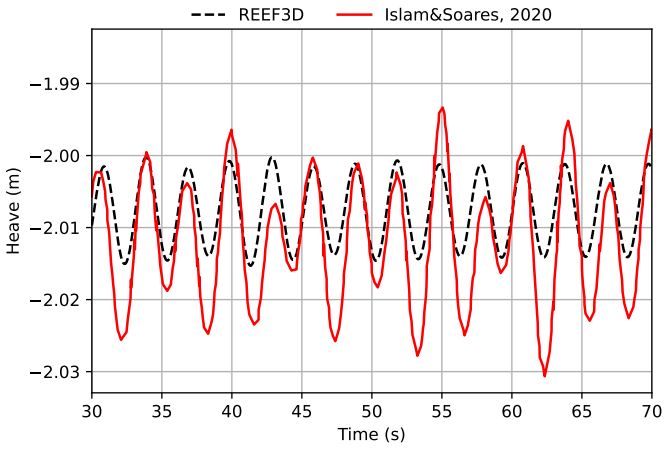

Figure 10: Comparison of the time history for the heave response,(T=3.0s, H=0.177 m and S=0.002).

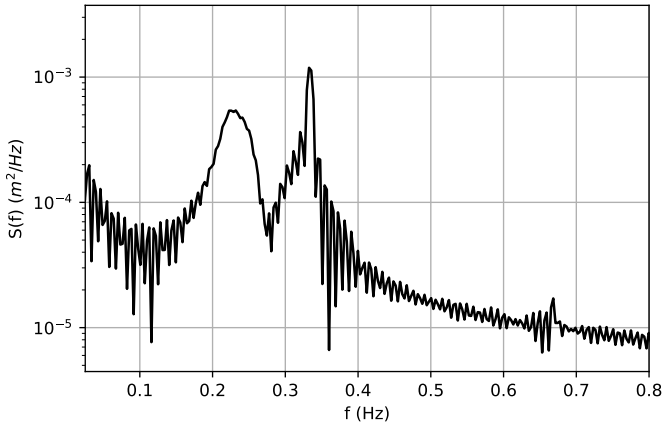

Figure 11: Power spectral density of the heave motion,(T=3.0s, H=0.177 m and S=0.002).

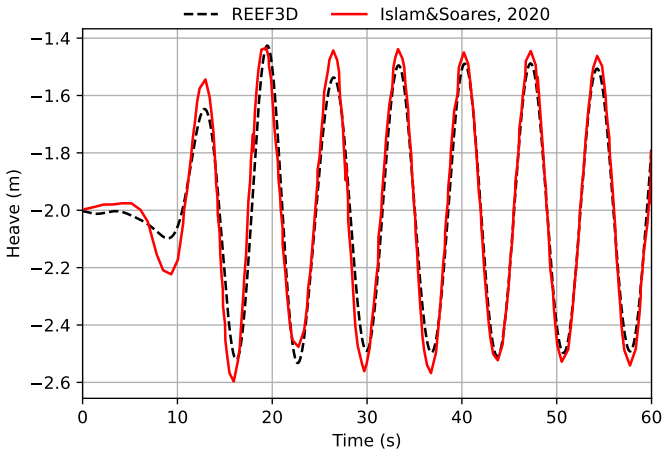

Figure 12: Comparison of the time history for the heave response,(T=7.0s, H=0.961 m and S=0.002).

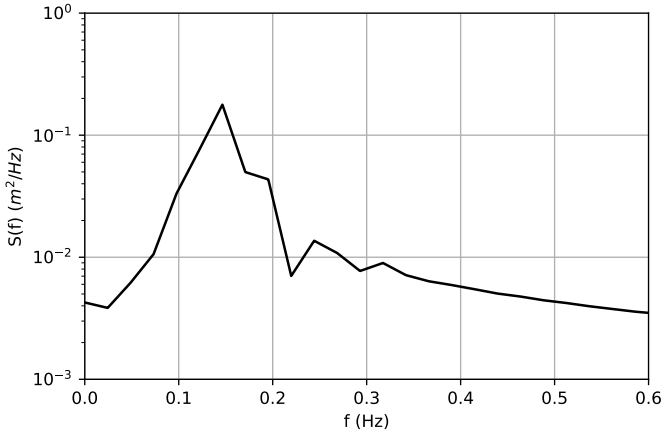

Figure 13: Power spectral density of the heave motion,(T=7.0s, H=0.961 m and S=0.002).

4 CONCLUSIONS

In this paper, the capability of a direct-forcing immersed boundary method which is implemented within the numerical hydrodynamic framework REEF3D has been investigated for a 3-dimensional having sphere. Numerical results have been compared with the available numerical results in the literature. Free-decay tests show that REEF3D predicts smaller motion amplitude in comparison to other tools which is needed to be investigated further. On the other hand, REEF3D is able to capture high-order wave radiation effects and breaking radiated waves, precisely. In addition, numerical findings from the wave simulations agree well with the other numerical result, and it is quite promising. For further studies, the other wave conditions also will be performed and the results will be presented.

REFERENCES

Aggarwal, A., M. A. Chella, H. Bihs, & Ø. A. Arntsen (2017). Numerical study of irregular breaking wave forces on a monopile for offshore wind turbines. *Energy Procedia 137*, 246–254.

Alagan Chella, M., H. Bihs, D. Myrhaug, & M. Muskulus (2017). Breaking solitary waves and breaking wave forces on a vertically mounted slender cylinder over an impermeable sloping seabed. *Journal of Ocean Engineering and Marine Energy 3*(1), 1–19.

Ashby, S. & R. Flagout (1996). A parallel mulitgrid preconditioned conjugate gradient algorithm for groundwater flow simulations. *Nuclear Science and Engineering Volume 124(1)*, 145–159.

Bihs, H., A. Kamath, M. Alagan Chella, & C. Pakozdi (2017). Complex geometry handling for a cartesian grid based solver. In *MekIT'17-Ninth national conference on Computational Mechanics*. International Center for Numerical Methods in Engineering (CIMNE).

Bihs, H., A. Kamath, M. A. Chella, A. Aggarwal, & Ø. A. Arntsen (2016). A new level set numerical wave tank with improved density interpolation for complex wave hydrodynamics. *Computers & Fluids 140*, 191–208.

Calderer, A., X. Guo, L. Shen, & F. Sotiropoulos (2018). Fluid–structure interaction simulation of floating structures interacting with complex, large-scale ocean waves and atmospheric turbulence with application to floating offshore wind

turbines. *Journal of Computational Physics 355*, 144–175.
Durbin, P. A. (2009). Limiters and wall treatments in applied turbulence modeling. *Fluid Dynamics Research 41*, 1–18.
Hossain, M. S. & W. Rodi (1980). Mathematical modeling of vertical mixing in stratified channel flow. *2nd Symposium on Stratified Flows, Trondheim, Norway*.
Islam, H. & C. Guedes Soares (2020). Validation study for a heaving sphere in waves. In *Developments in Renewable Energies Offshore*, pp. 88–95. CRC Press.
Jiang, G. & D. Peng (2000). Weighted ENO schemes for Hamilton Jacobi equations. *SIAM Journal of Scientific Computing Volume 21*, 2126–2143.
Jiang, G.-S. & C.-W. Shu (1996). Efficient implementation of weighted eno schemes. *Journal of computational physics 126*(1), 202–228.
Kamath, A., M. A. Chella, H. Bihs, & Ø. A. Arntsen (2016). Breaking wave interaction with a vertical cylinder and the effect of breaker location. *Ocean Engineering 128*, 105–115.
Kamath, A., G. Fleit, & H. Bihs (2019). Investigation of free surface turbulence damping in rans simulations for complex free surface flows. *Water 11*(3), 456.
Liu, Y., Q. Xiao, A. Incecik, C. Peyrard, & D. Wan (2017). Establishing a fully coupled cfd analysis tool for floating offshore wind turbines. *Renewable Energy 112*, 280–301.
Martin, T., T. A., & H. Bihs (2021). numerical framework for modelling the dynamics of open ocean aquaculture structures in viscous fluids. *Applied Ocean Research 106*, 102410.
Miquel, A. M., A. Kamath, M. Alagan Chella, R. Archetti, & H. Bihs (2018). Analysis of different methods for wave generation and absorption in a cfd-based numerical wave tank. *Journal of Marine Science and Engineering 6*(2), 73.
Naot, D. & W. Rodi (1982). Calculation of secondary currents in channel flow. *Journal of the Hydraulics Division, ASCE 108*(8), 948–968.
Osher, S. & J. A. Sethian (1988). Fronts propagating with curvature-dependent speed: Algorithms based on Hamilton-Jacobi formulations. *Journal of Computational Physics 79*, 12–49.
Peng, D., B. Merriman, S. Osher, H. Zhao, & M. Kang (1999). A PDE-based fast local level set method. *Journal of Computational Physics 155*, 410–438.
Shu, C. & S. Osher (1988). Efficient implementation of essentially non-oscillatory shock-capturing schemes. *Journal of Computational Physics Volume 77(2)*, 439–471.
Sussman, M., P. Smereka, & S. Osher (1994). A level set approach for computing solutions to incompressible two-phase flow. *Journal of Computational Physics 114*, 146–159.
Timmermans, L. J., P. D. Minev, & F. N. Van De Vosse (1996). An approximate projection scheme for incompressible flow using spectral elements. *International journal for numerical methods in fluids 22*(7), 673–688.
van der Vorst, H. (1992). BiCGStab: A fast and smoothly converging variant of Bi-CG for the solution of nonsymmetric linear systems. *SIAM Journal of Scientific Computing Volume 13*, 631–644.
Wang, G., T. Martin, L. Huang, & H. Bihs (2022). A numerical study of the hydrodynamics of an offshore fish farm using reef3d. *Journal of Offshore Mechanics and Arctic Engineering 144*(2), 021301.
Wendt, F. F., Y.-H. Yu, K. Nielsen, K. Ruehl, T. Bunnik, I. Touzon, B. W. Nam, J. S. Kim, C. E. Janson, K.-R. Jakobsen, et al. (2017). International energy agency ocean energy systems task 10 wave energy converter modeling verification and validation. Technical report, National Renewable Energy Lab.(NREL), Golden, CO (United States).
Wilcox, D. C. (1994). *Turbulence modeling for CFD*. DCW Industries Inc., La Canada, California.
Yang, L. (2018). One-fluid formulation for fluid–structure interaction with free surface. *Computer Methods in Applied Mechanics and Engineering 332*, 102–135.